Journal of Materials Chemistry B

Accepted Manuscript

ROYAL SOCIETY OF CHEMISTRY

www.rsc.org/materialsB

3D-Printed Magnetic Fe_3O_4/MBG/PCL Composite Scaffolds with Multifunctionality of Bone Regeneration, Local Anticancer Drug Delivery and Hyperthermia

Jianhua Zhang[a1], Shichang Zhao[b1], Min Zhu[c], Yufang Zhu[c]*, Yadong Zhang[b], Zhongtang Liu[d], Changqing Zhang[b]*

[a] School of Medical Instrument and Food Engineering, University of Shanghai for Science and Technology, 516 Jungong Road, Shanghai 200093, People's Republic of China.

[b] Department of Orthopaedics, Shanghai Sixth People's Hospital, Shanghai Jiaotong University, 600 Yishan Road, Shanghai 200233, People's Republic of China.

[c] School of Materials Science and Engineering, University of Shanghai for Science and Technology, 516 Jungong Road, Shanghai 200093, People's Republic of China.

[d] Department of Orthopaedics, Changhai Hospital, Second Military Medical University, 174 Changhai Road Shanghai 200433, People's Republic of China.

*Corresponding authors:

Prof. Yufang Zhu: Tel: +86-21-55271663; Email: zjf2412@163.com

Prof. Changqing Zhang: Tel: +86 21 64369181; Email: zhangcq@sjtu.edu.cn

[1] The first two authors contributed equally to this work.

Abstract: In this study, three-dimensional (3D) magnetic Fe_3O_4 nanoparticles containing mesoporous bioactive glass/polycaprolactone (Fe_3O_4/MBG/PCL) composite scaffolds have been fabricated by 3D-printing technique. The physiochemical properties, in vitro bioactivity, anticancer drug delivery, mechanical strength, magnetic heating ability and cell response to Fe_3O_4/MBG/PCL scaffolds were systematically investigated. The results showed that Fe_3O_4/MBG/PCL scaffolds had uniform macropores of 400 μm, high porosity of 60 % and excellent compressive strength of 13-16 MPa. The incorporation of magnetic Fe_3O_4 nanoparticles into MBG/PCL scaffolds did not influence their apatite mineralization ability, but endowed excellent magnetic heating ability and significantly stimulated proliferation, alkaline phosphatase (ALP) activity, osteogenesis-related gene expression (RUNX2, OCN, BSP, BMP-2 and Col-1) and extra-cellular matrix (ECM) mineralization of human bone marrow-derived mesenchymal stem cells (h-BMSCs). Moreover, using doxorubicin (DOX) as a model anticancer drug, Fe_3O_4/MBG/PCL scaffolds exhibited a sustained drug release for use in local drug delivery therapy. Therefore, the 3D-printed Fe_3O_4/MBG/PCL scaffolds showed the potential multifunctionality of enhanced osteogenic activity, local anticancer drug delivery and magnetic hyperthermia.

Keywords: 3D printing; Mesoporous bioactive glass; Fe_3O_4 nanoparticles; Magnetic hyperthermia; Bone regeneration

1. Introduction

Treatment of primary bone tumors and bone metastasis of malignant tumors is a major challenge in orthopedic surgery. The standard limb salvage treatment is anatomic and functional reconstruction after resection of the tumor, followed by postoperative radiation or chemotherapy [1]. However, these procedures are not always sufficient for tumor management, and the tumor recurrence and non-osseous union often occur. Successful reconstruction of bone defects caused by tumor resection and prevention of recurrence are the keys to improve the prognosis of patients with primary bone tumors or skeletal metastasis. To date, many strategies have been accepted to create a favorable microenvironment for repairing bone defects [2-8]. Among them, 3D porous biomaterial scaffolds act as a temporary framework, providing a suitable environment for cell adhesion, growth and phenotype maintenance, and thereby be beneficial for bone regeneration [4-8]. Traditional methods for fabricating 3D porous bone tissue scaffolds, such as polyurethane foam templating, solvent casting, melt molding and freeze drying are difficult to control the pore interconnection, pore size and overall porosity of the scaffolds [9-10]. Recently, a three-dimensional (3D) printing technique has been developed to overcome these problems for fabricating ideal scaffolds used for bone tissue engineering [11-12]. The significant advantage of this new method for bone-graft fabrication is that customized implants with precisely controlled architectures for large-size or geometrically complex bone defects resulted from tumor resection could be printed from Computer Assisted Design (CAD) based on computerized tomography (CT) or magnetic resonance imaging (MRI) 3D data files of patients. Therefore, it would be advantageous to have customized tissue

engineered bone grafts with anticancer property that simultaneously control tumor recurrence while promoting bone regeneration in order to avoid multiple surgeries and delayed reconstruction [13].

In the past few years, more attention has been paid to mesoporous bioactive glass (MBG) due to its efficient drug delivery and superior bone tissue regenerative capability [14-20]. Compared with non-mesoporous bioactive glasses (NBG), MBG possess more optimal surface area, nanopore volume, enhanced in vitro apatite mineralization in SBF, controlled drug delivery properties and in vivo bioactivity [14-18]. Recently, Wu et al. reviewed the advances of MBG materials, including the preparation of different forms of MBG, composition-structure relationship, efficient drug/growth factor delivery and bone tissue engineering application [19]. Vallet-Regĺ et al. also highlighted that MBG materials could be revisiting bioceramics for bone regeneration and local drug delivery systems [16]. Therefore, MBG materials could be promising as a multifunctional platform with bone regeneration and local anticancer drug delivery for repairing bone defects after tumor resection.

Due to their specific physical properties and excellent biocompatibility, magnetic Fe_3O_4 nanoparticles have been widely investigated for magnetic hyperthermia [21-23]. Exposed to an alternating magnetic field, magnetic Fe_3O_4 nanoparticles can generate heat due to the Néel and Brownian relaxations and hysteresis loss [24]. When the target tissues temperature is heated to 42–45 ^{o}C, cancerous cells are damaged or killed due to hemorrhage, stasis and vascular occlusion whereas normal cells survive [25]. Matsumine et al. prepared Fe_3O_4-containing calcium phosphate (Fe_3O_4–CaP) cement to treat patients with

metastatic bone lesions by hyperthermia treatment. The results demonstrated that patients treated with hyperthermia showed better radiographic outcomes than those treated with palliative operation [26]. Also, clinical applications of magnetic Fe_3O_4 nanoparticles for hyperthermia treatment of tumors have been conducted by MagForce Nanotechnologies AG, Berlin, Germany [27]. On the other hand, magnetic Fe_3O_4 nanoparticles containing biomaterials have also been of great interest in the field of bone tissue regeneration. Studies demonstrated that magnetic nanoparticles had the effect of osteoinduction even without external magnetic force [28-33]. For example, Huang et al reported that superparamagnetic iron oxide nanoparticles are not toxic to human mesenchymal stem cells (hMSCs), but instead promote cell proliferation and increase cell growth [28]. Wu et al demonstrated that the introduction of magnetic nanoparticles to Ca-P bioceramics could stimulate osteoblast cells adhesion, proliferation, and differentiation in vitro and promote bone formation and growth in vivo [31]. Meng et al demonstrated that the addition of magnetic nanoparticles in hydroxyapatite nanoparticles (nHA)/poly (D, L-lactide) (PLA) composite nanofibrous scaffolds could accelerate proliferation and differentiation of pre-osteoblast cells and in vivo osteogenesis in a lumbar transverse defect model of New Zealand white rabbits [32-33].

The innovative concept of surgical implantation of high osteogenic scaffolds with tailored hierarchical meso-macroporosity followed by concurrent anti-cancer drug chemotherapy and local magnetic hyperthermia could provide a new strategy for bone tumor therapy. The aims of this study were to fabricate multifunctional magnetic Fe_3O_4/MBG/PCL composite scaffolds by a 3D printing method, and systematically

investigate the effects of magnetic Fe_3O_4 nanoparticles on the physicochemical properties of MBG/PCL scaffolds, and the morphology, proliferation, ALP activity, osteogenesis–related gene expression and ECM mineralization of h-BMSCs attached to the scaffolds. Furthermore, the anticancer drug delivery property and magnetic heating ability of Fe_3O_4/MBG/PCL scaffolds were also evaluated.

2. Materials and methods

2.1 Materials

Nonionic block copolymer $EO_{20}PO_{70}EO_{20}$ (P123, Mw = 5800) was purchased from BASF. Hydrochloric acid (HCl, ⩾36 %), tetraethyl orthosilicate (TEOS, 98 %), triethyl phosphate (TEP, 99.8 %), Ethanol(99.7 %)and calcium nitrate ($Ca(NO_3)_2 \cdot 4H_2O$,99 %)were purchased from Sinopharm Chemical Reagent Co. Ltd. Iron Chloride hexahydrate ($FeCl_3 \cdot 6H_2O$, 99 %), iron dichloride tetrahydrate ($FeCl_2 \cdot 4H_2O$,99 %) and Sodium hydroxide(NaOH, 96 %)was purchased from Aibi Chemistry Preparation Co. Ltd. Doxorubicin hydrochloride (DOX, 98 %), Polycaprolactone (PCL,Mn70000-90000) was purchased from Sigma-Aldrich. All chemicals were used without further purification.

2.2 Preparation of MBG powder and magnetic Fe_3O_4 nanoparticles

MBG powders (Si/Ca/P molar ratio 80/15/5) were prepared by using nonionic block copolymer $EO_{20}PO_{70}EO_{20}$ (P123) as a structure-directing agent, according to the previously reported method [14]. In a typical synthesis, 4.0 g of P123, 6.7 g of tetraethyl orthosilicate (TEOS), 1.4 g of $Ca(NO_3)_2 \cdot 4H_2O$, 0.73 g of triethyl phosphate (TEP) and 1.0 g of 0.5 M HCl were dissolved in 60 g of ethanol and stirred at room temperature for 24 h. The resulting sol was introduced into a Petri dish for evaporation-induced self-assembly (EISA) for 24 h, and

then the dry gel was calcined at 600 ^{o}C for 5 h to obtain MBG powders.

Magnetic Fe_3O_4 nanoparticles were obtained by a co-precipitation method with some modification, according to the previously reported method [34]. As an example, 5.2 g of $FeCl_3 \cdot 6H_2O$, 3.825 g of $FeCl_2 \cdot 4H_2O$ and 0.85 ml of hydrochloric acid (HCl, ⩾36 %) were dissolved in 25 ml of deionized water. Subsequently, 250 ml of NaOH solution (1.5 M) was added dropwise under vigorous stirring. The supernatant solution was discarded and the precipitate washed with 100 ml of deionized water under sonication. The centrifugation and washing steps were repeated three times. Finally, the resultant precipitate was dried at 60 ^{o}C in vacuum oven for 24h.

2.3 Preparation of Fe_3O_4/MBG/PCL scaffolds by 3D printing

In this study, the 4th 3D Bioplotter™ (EnvisionTEC GmbH, Germany) was used to print 3D scaffolds. Before printing the scaffolds, the injectable Fe_3O_4/MBG/PCL paste was prepared as follows. Firstly, the MBG powders and magnetic Fe_3O_4 nanoparticles were ground and passed through 400 mesh sieves, resulting in a particle size of less than 37 μm. The 0.8 g of Fe_3O_4/MBG mixed powder, where either no Fe_3O_4 or 5 wt% or 10 wt% or 15 wt% of Fe_3O_4 was replaced for MBG, were named as MBG, 5Fe_3O_4/MBG, 10Fe_3O_4/MBG and 15Fe_3O_4/MBG. Subsequently, 0.5 g of PCL was completely dissolved in 2 ml of chloroform. The Fe_3O_4/MBG mixed powder were added to the PCL solution ($W_{Fe_3O_4/MBG}$: W_{PCL}= 62:38), and the mixture was quickly stirred at room temperature until it had formed a paste for injection. Finally, the prepared paste was introduced into a polyethylene injection cartridge that was fixed onto the 3D Bioplotter™ printing device.

Simultaneously, square block models (6×6×6mm) were loaded on the Bioplotter

CAD/CAM software and scaffold was plotted by layer-by-layer, through the extrusion of the paste as a fiber, up to 29 layers. The architecture was changed by plotting fibers with 0 and 90 angle steps between two successive layers, the dosing pressure to the syringe pump was 1.5-3.0 bar and the speed of the dispensing unit was 1.5-5 mm/s, the nozzle size was 0.25 mm. Finally, the obtained Fe_3O_4/MBG/PCL scaffolds were dried in an oven at 37 ^oC for 2 days to evaporate the chloroform.

2.4 Characterization of MBG powder, magnetic Fe_3O_4 nanoparticles and Fe_3O_4/MBG/PCL scaffolds

The wide-angle XRD patterns were obtained on a Bruker D8 advance. Scanning electron microscopy (SEM) was carried out with a FEI Quanta 450 field emission scanning electron microscope. Transmission electron microscopy (TEM) was performed with a JEM-2010 electron microscope operated at an acceleration voltage of 200 kV. N_2 adsorption–desorption isotherms were obtained on a Micromeritics Tristar 3020 at -196 ^oC under continuous adsorption conditions. Brunauer-Emmett-Tellwe (BET) and Barrett-Joyner-Halenda (BJH) methods were used to determine the surface area and the pore size distribution. Magnetization curves were conducted on a Nanjing Nanda LH-3 Vibrating Sample Magnetometer.

The porosity of Fe_3O_4/MBG/PCL scaffolds (6×6×6mm) was measured using Archimedes' principle. Water was used as liquid medium. The porosity (P) was calculated according to the following formulation: $P = \frac{W_{sat} - W_{dry}}{W_{sat} - W_{sus}} \times 100\%$, where W_{dry} is the dry weight of Fe_3O_4/MBG/PCL scaffolds, W_{sus} is the weight of Fe_3O_4/MBG/PCL scaffolds suspended in

water and W_{sat} is the weight of Fe_3O_4/MBG/PCL scaffolds saturated with water.

The compressive strength of Fe/MBG/PCL scaffolds (6×6×6 mm) was tested using a Zwick static materials testing machine (5 KN) at a cross-head speed of 0.5 mm min^{-1}. Five samples were used for replicates of this experiment.

2.5 Ion dissolution and apatite formation of Fe_3O_4/MBG/PCL scaffolds in simulated body fluids

To investigate the ion dissolution from Fe_3O_4/MBG/PCL scaffolds, simulated body fluid (SBF) with ion concentrations similar to those in human blood plasma was prepared according to the method described by Kokubo [35]. Fe_3O_4/MBG/PCL scaffolds were soaked in SBF at 37 ^oC for 1, 3, 5 and 7 days, at 200 ml/g of solution volume to scaffold mass, in accordance with previous report [36]. After soaking, Fe_3O_4/MBG/PCL scaffolds were collected from SBF solution, rinsed with ethanol and distilled water and then dried at 37 ^oC. The apatite formation on the surfaces of Fe_3O_4/MBG/PCL scaffolds was confirmed by SEM and energy-dispersive X-ray spectroscopy (EDS) analysis. The concentrations of Si, Ca, Fe and P ions in SBF solution at predetermined time intervals were determined by inductively coupled plasma optical emission spectroscopy (ICP-OES, Perkin Elmer Optima7000DV). The pH values of SBF solution were tested after soaking Fe_3O_4/MBG/PCL scaffold at predetermined time intervals. Three samples were used for replicate experiments.

2.6 Drug loading and release from Fe_3O_4/MBG/PCL scaffolds

In this study, doxorubicin hydrochloride (DOX), an anti-cancer drug, was selected to examine the drug loading and delivery property of Fe_3O_4/MBG/PCL scaffolds. DOX is a small molecule, and can thus possibly transport into the mesopore channels (3-5 nm). Typically,

DOX was dissolved in phosphate buffered saline (PBS) at a concentration of 0.25 mg/ml to evaluate the drug loading properties. Firstly, 2 g of MBG powders was immersed in 20 ml of DOX solution under gentle stirring for 24 h. The DOX-loaded MBG powders were collected by centrifugation and dried at 37 ^{o}C in a vacuum oven for 24 h. Then, the DOX-loaded MBG powders were used to fabricate Fe_3O_4/MBG/PCL scaffolds by 3D printing.

The estimation of DOX loaded in MBG powders was carried out by measuring the absorbance values at 481 nm before and after loading using UV-vis analysis. Before determination, a calibration curve was recorded by NanoDrop 2000C Spectrophotometer. DOX release was evaluated by placing the DOX-loaded Fe_3O_4/MBG/PCL scaffolds into phosphate buffered saline (PBS, pH=7.4) with $V_{SBF}/M_{scaffold}$ of 100 ml/g at 37 ^{o}C for 12, 24, 48, 96, 120, 144, 168, 192and 216 h. DOX release was determined by NanoDrop 2000C Spectrophotometer. The cumulative release of DOX (%) was calculated with the equation: DOX (%) = (total DOX released/total loading of DOX in scaffolds)×100 %. Three samples were used for replicate experiments and UV analysis for drug release was carried out three times for each sample.

2.7 Magnetic heating property of Fe_3O_4/MBG/PCL scaffolds

Magnetic heating property of Fe_3O_4/MBG/PCL scaffolds was evaluated using a DM100 System (nB nanoScale Biomagnetics, Spain) and the temperature was measured with an optical fiber temperature sensors. The ground magnetic scaffolds powder was dispersed in water to a concentration of 10 mg/mL. The solution (1.0 ml) was heated in an alternating magnetic field of 180 G in strength at 409 kHz frequency for 30 min. The upper limited temperature was set up 80 ^{o}C. The capacity of a magnetic material to absorb energy from

an alternating magnetic field is quantified through the SAR index.

2.8 Cell attachment and proliferation on Fe_3O_4/MBG/PCL scaffolds

Primary human bone marrow-derived mesenchymal stem cells (h-BMSCs) were isolated as previously described [37]. The use of human samples was approved by the ethical committee of Sixth People's Hospital, Shanghai Jiaotong University School of Medicine. In brief, bone marrow (approximately 7 mL) was carefully collected into polypropylene tubes containing preservative-free heparin (1000 U/mL). Then, the marrow was suspended in Dulbecco' s Modified Eagle' s Medium (DMEM) containing 4.5 g/L glucose (Gibco, Carlsbad, CA), supplemented with 10% fetal bovine serum (FBS), and antibiotics (penicillin G, 100 U/mL; and streptomycin 0.1 mg/mL). The cells were plated into dishes and incubated at 37 ^{o}C in a humidified atmosphere with 5% CO_2. Non-adherent cells were removed by changing the culture medium after 5 days of incubation. After 10 days of primary culture, the cells were detached and serially subcultured in 25 cm^2 flasks. The medium was changed every 2-3 days. Cells were detached with 0.25 % trypsin, 0.1 % EDTA and passaged at 80 % confluence. Cells at the fifth passage were used for subsequent experiments.

In order to assess cell adhesion and details of cell/biomaterial interaction, 1×10^5 h-BMSCs were cultured on each Fe_3O_4/MBG/PCL scaffold (MBG/PCL, $5Fe_3O_4$/MBG/PCL, $10Fe_3O_4$/MBG/PCL and $15Fe_3O_4$/MBG/PCL) in 24-well culture plate. The cells were then incubated in DMEM (GIBCO, Invitrogen Pty Ltd., Australia) culture medium supplemented with 10 % fetal calf serum (FCS; InVitro Technology, Australia) in humidified culture conditions. After 7days, the samples were removed from the culture wells, rinsed with PBS,

fixed with 2.5 % glutaraldehyde in PBS for 1 h. The fixative was removed by washing with buffer containing 4 % (w/v) sucrose in PBS and post fixed in 1 % osmium tetroxide in PBS followed by sequential dehydration in graded ethanol (50 %, 70 %, 90 %, 95 %, 100 %) and hexamethyldisilizane (HMDS). The specimens were coated with gold and the morphological characteristics of the attached cells determined using SEM (FEI Quanta 450).

In order to investigate the proliferation of h-BMSCs on four different types of Fe_3O_4/MBG/PCL scaffold, Cell Counting Kit-8 assay (CCK-8, Dojindo) were used. Briefly, h-BMSCs were cultured on scaffolds at an initial density of 10^4cells/ scaffold for 1, 3 and 7 days. Then 400ul of culture medium and 40ul CCK-8 solution was added to each well at each time point and incubated at 37 ^oC for another 4 h. An aliquot of 100ul was taken from each well and transferred to a fresh 96 well plate. The light absorbance of these samples was measured at 450 nm with a spectrophotometric microplate reader (Bio-Rad 680, USA).All the results were expressed as the optical density values minus the absorbance of blank wells.

2.9 ALP activity and osteogenic related gene expression of h-BMSCs cells on Fe_3O_4/MBG/PCL scaffolds

The procedure was performed according to a previous study [38]. To assess the development of the osteoblastic phenotype of h-BMSCs grown on various types of Fe_3O_4/MBG/PCL scaffolds, ALP activity was performed on day 7 and 14 after seeding 1×10^5 h-BMSCs on each scaffold (n = 3) from different groups. All the experiments were done in triplicate in 24-well culture plates. At the predetermined time point, culture medium was decanted and cell layer washed gently three times with PBS followed by washing once in cold 50 mM Tris buffer, and then h-BMSCs were lysed in 200 µl 0.2 % Triton X-100. Lysates

were sonicated after being centrifuged at 14,000 rpm for 15 min at 4 ^{o}C. 50 µl supernatant was mixed with 150 µl working solution according to the manufacturer's protocol (Beyotime). The conversion of p-nitrophenylphosphate into p-nitrophenol in the presence of ALP was determined by measuring the absorbance at 405 nm with a microplate reader (Bio-Rad 680, USA). The ALP activity was calculated from a standard curve after normalizing to the total protein content and the results expressed in mM of p-nitrophenol produced per minute per milligram of protein.

The expression levels of osteogenesis related genes (runt-related transcription factor 2 (RUNX2), osteocalcin (OCN), bone sialoprotein (BSP), bone morphgenetic protein-2 (BMP-2) and collagen type I (COL1)) were measured using the qRT-PCR. The cells were seeded at a density of 2×10^4 cells/well, cultured for 14 days and harvested using TRI zol Reagent (Invitrogen Pty Ltd., Australia) to extract the RNA. The obtained RNA was reverse transcribed into complementary DNA (cDNA) using RevertAid First Strand cDNA Synthesis Kit (Thermo) and the qRT-PCR analysis was performed on an ABI Prism 7300 Thermal Cycler (Applied Biosystems, Australia) using SYBR Green detection reagent. The relative expression of the genes of interest was normalized against the housekeeping gene GAPDH. All samples were assayed in triplicate and independent experiments were performed. The mean cycle threshold (Ct) value of each target gene was normalized against the Ct value of GAPDH. The relative expression was calculated using the following formula: $2^{-(\text{normalized average Ct}) \times 100}$.

2.10 ECM mineralization of h-BMSCs cells on Fe_3O_4/MBG/PCL scaffolds

The ability of Fe_3O_4/MBG/PCL scaffolds to support mineralization by the h-BMSCs was studied using the Alizarin red S assay (Genmed Scientifics Inc., U.S.A), as previously

described [32].After 14 days culture, cells on Fe/MBG/PCL scaffolds were rinsed with PBS for 3 times and fixed in 4 % (w/v) paraformaldehyde (PFA) for 15 min at room temperature and stained for 15 min with 2 % (w/v) Alizarin Red S solution at pH 4.2. The cells were washed extensively with distilled water and viewed under a phase contrast light microscope.

2.11 Statistical analysis

The data were collected from three separate experiments and expressed as means ± standard deviation. The one way ANOVA and Student-Newman-Keuls post hoc tests were used to determine the level of significance and p values less than 0.05 were considered to be significant.

3. Results

3.1 Characterization of MBG powders and Fe_3O_4/MBG/PCL scaffolds

As shown in TEM image (Fig. 1A), MBG powder had highly ordered two dimensional hexagonal mesoporous channels. Wide-angle XRD analysis in Fig. 1B showed MBG powder had no diffraction peaks appearing on the patterns except for a broad reflection at $2\theta = 15 - 30^{o}$, suggesting the amorphous phase of MBG powder. Fig. 1C shows N_2 adsorption–desorption isotherm of MBG powders together with the corresponding pore size distribution. The type IV isotherm with a type H1 hysteresis loop (Fig. 1C) indicated the *P6mm* mesoporous structure of MBG materials. The BET surface area and pore volume at P/P_0= 0.97 for MBG powders were 403 m^2/g and 0.49 cm^3/g, respectively. The pore size distribution of MBG powders calculated from the desorption branch using the BJH model is

narrow, and peaked at 3.5 nm (insert of Fig. 1C). These results are similar to the previously reported MBG materials [18]. MBG powders were ground and passed through 400 mesh sieves, which suggests that the particle size of MBg powders was less than 37 μm. Fe_3O_4 nanoparticles had small particle sizes ranged from 15 to 20 nm (Fig. 1D), indicating the superparamagnetic behavior, because magnetic Fe_3O_4 particles exhibit superparamagnetic behavior when the particle size decreases to below a critical value, generally around 20 nm [39].

Photograph and SEM observation in Fig.2 showed that the MBG/PCL, $5Fe_3O_4$/MBG/PCL, $10Fe_3O_4$/MBG/PCL and $15Fe_3O_4$/MBG/PCL scaffolds with 0 and 90 angle steps between two successive layers and regular macroporous structure were successfully fabricated by the 4th 3D Bioplotter™. The macropore size was close to 400 μm. Furthermore, it can be seen that the $5Fe_3O_4$/MBG/PCL, $10Fe_3O_4$/MBG/PCL and $15Fe_3O_4$/MBG/PCL scaffolds were attracted on the bottom of the magnet and did not drop down, suggesting that those scaffolds except MBG/PCL scaffolds have magnetic behaviors. On the other hand, the surfaces of each type of scaffolds were smooth, and very small amount of powders can be observed on the surfaces, but the powders were embedded in PCL matrix. The porosities of the MBG/PCL, $5Fe_3O_4$/MBG/PCL, $10Fe_3O_4$/MBG/PCL and $15Fe_3O_4$/MBG/PCL scaffolds were estimated at 59.6±5.6 %, 62.9±6.7 %, 61.7±5.4 % and 61.7±5.4 %, respectively (Table 1). As shown in Fig. 2C, the compressive strength of the MBG/PCL, $5Fe_3O_4$/MBG/PCL, $10Fe_3O_4$/MBG/PCL and $15Fe_3O_4$/MBG/PCL scaffolds were 13.1±1.6 MPa, 13.9±1.4 MPa, 15.7±4.0 MPa and 16.6±1.9 MPa, respectively. After soaking in SBF for 7 days, the MBG/PCL, $5Fe_3O_4$/MBG/PCL, $10Fe_3O_4$/MBG/PCL and $15Fe_3O_4$/MBG/PCL scaffolds maintained high compressive strength,

which were 10.9±0.6 MPa, 11.8±0.3 MPa, 13.2±0.8 MPa and 14.0±1.0 MPa, respectively. Fig. 2D shows wide-angle XRD patterns of Fe_3O_4 nanoparticles, polycaprolactone (PCL) and Fe_3O_4/MBG/PCL scaffolds. When Fe_3O_4, MBG and PCL were mixed to form Fe_3O_4/MBG/PCL scaffolds, characteristic diffraction peaks of Fe_3O_4 and PCL were observed on the patterns, but broad reflection of MBG at $2\theta = 15 - 30^{o}$ was overlapped with those of PCL. For the Fe_3O_4/MBG/PCL scaffolds, a positive correlation between the diffraction intensities of Fe_3O_4 and Fe_3O_4 content in the scaffolds can be observed. On the other hand, there were no significant changes in the phase structures when Fe_3O_4, MBG and PCL were mixed, suggesting that there was little chemical reaction among Fe_3O_4, MBG and PCL composites.

3.2 Ion dissolution and apatite mineralization ability of Fe_3O_4/MBG/PCL scaffolds

Fig. 3 shows the dissolutions of Si, Ca and P ions and pH changes in SBF after soaking Fe_3O_4/MBG/PCL scaffolds for different periods. It can be seen that the concentration changes of Ca, Si and P ions for all of scaffolds are close to each other. The Si concentrations increased with increasing soaking time, while both Ca and P concentrations increased at the early soaking stage, and decreased after 3 days. With increasing soaking time, the pH values in the scaffold-soaked SBF increased within two days, and followed by a stable level thereafter. However, the scaffolds with high Fe_3O_4 content showed lower pH value.

SEM images and EDS analysis for magnetic Fe_3O_4/MBG/PCL scaffolds before and after soaking in SBF for 3 days were shown in Fig. 2 and Fig. 4. SEM analysis showed that before soaking in SBF, the surface morphologies of four Fe_3O_4/MBG/PCL scaffolds were smooth (Fig. 2 E2, F2, G2 and H2). After soaking for 3 day, some petals nanoparticles were deposited on

the surface of those scaffolds due to the mineralization of Fe_3O_4/MBG/PCL scaffolds in SBF (Fig. 4). The morphologies of these mineralized apatite particlels show no obvious difference among the MBG/PCL, 5Fe_3O_4/MBG/PCL, 10Fe_3O_4/MBG/PCL and 15Fe_3O_4/MBG/PCL scaffolds (Fig. 4 A2, B2, C2 and D2). EDS analysis was used to confirm the surface compositions of four scaffolds after soaking in SBF for 3 days (Fig. 4 A3, B3, C3 and D3). There were obvious characteristic peaks for Ca and P elements on each EDS spectrum, and the Ca/P ratio of the MBG/PCL, 5Fe_3O_4/MBG/PCL, 10Fe_3O_4/MBG/PCL and 15Fe_3O_4/MBG/PCL scaffolds was 1.46, 1.65, 1.35 and 1.42, respectively, which are close to the Ca/P ratio of 1.67 for apatite, indicating the apatite mineralization on the surfaces of Fe_3O_4/MBG/PCL scaffolds.

3.3 DOX release from Fe_3O_4/MBG/PCL scaffolds

In this study, DOX, an anti-cancer drug, was used as a model drug to monitor the drug loading and release kinetics of the Fe_3O_4/MBG/PCL scaffolds. DOX loading efficiencies of the MBG powders was estimated at 84.8 ± 5.0%. Fig. 5 shows DOX release profiles from MBG/PCL, 5Fe_3O_4/MBG/PCL, 10Fe_3O_4/MBG/PCL and 15Fe_3O_4/MBG/PCL scaffolds in SBF at 37 ^{o}C. Each type of Fe_3O_4/MBG/PCL scaffolds exhibited similar sustained release behaviors throughout the whole study period. About 30 % of the loaded DOX was released from the scaffolds during the first day, and followed by a relatively slow release up to 10 days.

3.4 Magnetic heating ability of Fe_3O_4/MBG/PCL scaffolds

The magnetization curves of the Fe_3O_4/MBG/PCL scaffolds are shown in Fig. 6A. The

Fe_3O_4/MBG/PCL scaffolds exhibited superparamagnetic behavior due to no hysteresis loop. The magnetization saturation of the Fe_3O_4/MBG/PCL scaffolds increased with increasing Fe_3O_4 content, and the magnetization of MBG/PCL, 5Fe_3O_4/MBG/PCL, 10Fe_3O_4/MBG/PCL and 15Fe_3O_4/MBG/PCL scaffolds were 0, 1.01, 2.02 and 2.90 emu/g, respectively.

Fig. 6B shows the temperature changes in the surrounding environment of the scaffolds measured in an alternating magnetic field (180 G in strength and 409 kHz at frequency). In the alternating magnetic field, the solution temperature of MBG/PCL scaffolds did not increase, whereas the solution temperatures of 5Fe_3O_4/MBG/PCL, 10Fe_3O_4/MBG/PCL and 15Fe_3O_4/MBG/PCL scaffolds increased rapidly. The 15Fe_3O_4/MBG/PCL scaffolds induced the temperature increase from 20 ^{o}C to 43 ^{o}C at the AC frequency of 409 kHz and magnetic strength of 180 G within 2 min. Furthermore, the scaffolds showed a positive correlation between heating rate and Fe_3O_4 content in the scaffolds. The SAR index of the MBG/PCL, 5Fe_3O_4/MBG/PCL, 10Fe_3O_4/MBG/PCL and 15Fe_3O_4/MBG/PCL scaffolds were 0, 1.4, 2.9 and 4.7 W/g, respectively (Table 1).

3.5 Morphology, proliferation, ALP activity and osteogenic-related gene expression of h-BMSCs on Fe_3O_4/MBG/PCL scaffolds

The adhesion and morphology of h-BMSCs on the top surfaces of different Fe_3O_4/MBG/PCL were characterized by SEM observation (Fig. 7). After 7 days of culture, h-BMSCs attached to the surface of the pore walls and penetrated inside the pore structure presenting well-spread morphology (numerous filopodia) on all type of scaffolds (Fig. 7). However, more h-BMSCs were observed on the 5Fe_3O_4/MBG/PCL, 10Fe_3O_4/MBG/PCL and

$15Fe_3O_4$/MBG/PCL scaffolds than the MBG/PCL scaffolds.

The proliferation of h-BMSCs cultured on Fe_3O_4/MBG/PCL scaffolds was determined by CCK-8 proliferation assay for 1, 3 and 7 days (Fig. 8A). During the culture time, all the fabricated scaffolds supported h-BMSCs proliferation, and no significant difference was found among the four type of scaffolds on day 1 and 3 ($P>0.05$). However, the proliferation rates on the $10Fe_3O_4$/MBG/PCL and $15Fe_3O_4$/MBG/PCL scaffolds were significantly higher than that on MBG/PCL scaffolds on day 7 ($P< 0.05$). As shown in Fig. 8B, there were no statistically significant differences in ALP activity of the h-BMSCs among all testing groups at day 7, but $5Fe_3O_4$/MBG/PCL, $10Fe_3O_4$/MBG/PCL and $15Fe_3O_4$/MBG/PCL scaffolds enhanced the osteoblast phenotype expression of h-BMSCs at day 14 compared to the MBG/PCL scaffolds ($P<0.05$), and also exhibited a positive correlation between ALP activity and Fe_3O_4 content of the scaffolds.

Similar to the ALP activity results, gene expression analysis showed that the incorporation of Fe_3O_4 nanoparticles into MBG/PCL scaffolds significantly enhanced osteogenic differentiation of h-BMSCs throughout the assay period. For RUNX2, OCN, BSP, BMP-2 and Col-1 mRNA expression, the expression levels on the $5Fe_3O_4$/MBG/PCL, $10Fe_3O_4$/MBG/PCL and $15Fe_3O_4$/MBG/PCL scaffolds were higher than those on the MBG/PCL scaffolds at day 7 and 14, and the $15Fe_3O_4$/MBG/PCL scaffolds exhibited the highest expression levels (Fig. 9).

3.6 ECM mineralization of h-BMSCs on Fe_3O_4/MBG/PCL scaffolds

ECM mineralization of h-BMSCs on Fe_3O_4/MBG/PCL scaffolds for 14 days was

determined by the Alizarin red S assay (Fig. 10). Many more ECM mineralized nodules were observed on the 5Fe_3O_4/MBG/PCL, 10Fe_3O_4/MBG/PCL and 15Fe_3O_4/MBG/PCL scaffolds than the MBG/PCL scaffolds, suggesting the higher calcium content of h-BMSCs cultured on the 5Fe_3O_4/MBG/PCL, 10Fe_3O_4/MBG/PCL and 15Fe_3O_4/MBG/PCL scaffolds than the MBG/PCL scaffolds.

4. Discussion

In this study, we have first successfully fabricated the ternary component (Fe_3O_4/MBG/PCL) magnetic composite scaffolds for bone tissue engineering using a 3D printing technique. 3D printing technique is used to control the pore size and pore morphology of the scaffolds as well as the strut. MBG combines excellent bioactivity and local drug delivery due to mesoporous structure. Fe_3O_4 nanoparticles provide thermoseeds for potential local hyperthermia and could stimulate osteoblast cell response to biomaterials. Polycaprolactone (PCL), a USA Food and Drug Administration (FDA)-approved biodegradable and biocompatible polymer, which has been widely used in clinical applications, such as prosthetic devices, implants, tissue-engineered skin and drug-delivery systems [40-43], can be used as the binder to fabricate Fe_3O_4/MBG/PCL scaffolds. The results showed that the pore size of MBG powder was about 3.5 nm, the Fe_3O_4/MBG/PCL scaffolds had a regular and uniform square macropore structure with 400 μm of macropore size and 60 % of porosity (Fig.1 and Fig.2 and Table 1) .In general, the hierarchical pore architecture and high porosity of the scaffolds are of great importance for bone tissue engineering applications. Pore sizes larger than 100 μm enable cell seeding, tissue

ingrowths and vascularization. Nanopores in the microporous (<2 nm) or mesoporous (2–50 nm) range allow for molecule transport for any nutrition, waste removal and signaling, and promote cell adhesion and adsorption of biological agents [44-45]. Therefore, the 3D printed Fe_3O_4/MBG/PCL scaffolds had desirable hierarchical pore structure for bone regeneration.

Importantly, the 3D printed magnetic Fe_3O_4/MBG/PCL scaffolds exhibited a high compressive strength of 13-16 MPa (Fig. 2C), which is much higher than the 3D plotted PCL scaffolds (5-6 MPa) [46] and pure MBG scaffolds (55 kPa)[18], and can match the requirement of human trabecular bone (2-12 MPa). Furthermore, after soaking in SBF for 7 days, the 3D printed magnetic scaffolds could maintain 10-13 MPa of compressive strength. The enhanced mechanical strength may be attributed to the PCL binder, which binds the MBG powders and Fe_3O_4 nanoparticles together to decrease the brittleness and improve their toughness of Fe_3O_4/MBG/PCL scaffolds. In addition, scaffolds prepared by 3D printing technique resulted in a more uniform and continuous pore structure, facilitating the improvement of the mechanical strength [36]. On the other hand, MBG can fast degrade in physiological environment, but the released Ca and P ions form the apatite layer on the surface of the scaffolds, and PCL polymers have a slow degradation rate in aqueous solution at 37 ^{o}C. Thus, the Fe_3O_4/MBG/PCL scaffolds would not lose mechanical strength quickly, which is beneficial for bone repair.

The apatite layer forming on the surface of biomaterials in physiological fluid could enhance the osteoblastic activity, including proliferation and differentiation, and predict the in vivo bone bioactivity [47]. Our study shows that the 3D printed magnetic Fe_3O_4/MBG/PCL

scaffolds possess excellent apatite mineralization ability in SBF (Fig. 4) and there were no apparent differences among the MBG/PCL, 5Fe_3O_4/MBG/PCL, 10Fe_3O_4/MBG/PCL and 15Fe_3O_4/MBG/PCL scaffolds, indicating that the incorporation of small amounts of magnetic Fe_3O_4 nanoparticles into MBG/PCL scaffolds does not inhibit their bioactivity, and thereby would be beneficial for bonding to living bone well when implanted in vivo.

Another significant advantage of the Fe_3O_4/MBG/PCL scaffolds is their drug delivery property. Controlled drug release property is one of the important factors for modern regenerative medicine [48]. Local anticancer drug delivery has the potential to increase the intratumoral drug concentration, and thereby enhance the therapeutic efficiency, which is more advantageous than traditional systemic chemotherapy treatment [49]. Due to high drug-loading capacity and sustained release properties of mesoporous channels, mesoporous bioactive materials are crucial for the efficient delivery of drugs [50-51]. In this study, DOX was chosen as a pharmacologic model for drug loading and delivery. The results showed that each type of Fe_3O_4/MBG/PCL scaffolds exhibited similar sustained release behaviors. The release kinetics clearly shows a two-stage behavior: an initial rapid release up to 24 h followed by a slow sustained release. It might be that the initial rapid release primarily resulted from the DOX molecules adsorbed on the outer surface or the outermost region of the scaffolds. While the slower release stage may be considered to reflect the release of the DOX that was inside the mesoporous channels. On the other hand, each type of scaffolds exhibited a close release rate, which might be that MBG determined the DOX release kinetics. Therefore, the results indicated that the 3D printed Fe_3O_4/MBG/PCL scaffolds could deliver anticancer drugs with sustained release behavior for chemotherapy.

Magnetic Fe_3O_4 nanoparticles possess unique properties for cancer treatment by hyperthermia therapy, because they are able to generate local heat due to the Néel and Brownian relaxations and hysteresis losses under an alternating magnetic field [52-54]. Recently, magnetic bioactive composites for bone tumor treatment are paid more attention. Da et al. reported that magnetic bioactive glass ceramics had potential to be used as thermoseeds for hyperthermia [55]. Matsuoka et al. developed magnetic cationic liposomes based on Fe_3O_4 nanoparticles and investigated in vivo efficacy for hyperthermia treatment of hamster osteosarcoma. Magnetoliposomes were injected directly into the osteosarcoma and then subjected to an alternating magnetic field. When the tumor was heated above 42 ^{o}C, complete tumor regression was observed in all of the treated hamsters [56]. In this study, Fe_3O_4/MBG/PCL scaffolds possess excellent magnetic hyperthermia property due to the incorporation of magnetic Fe_3O_4 nanoparticles. The solution temperature of 15Fe_3O_4/MBG/PCL scaffolds could increase from 20 ^{o}C to 43 ^{o}C within 2 min in the alternating magnetic field (Fig. 6B). On the other hand, studies demonstrated that magnetic Fe_3O_4 nanoparticles could be as thermoseeds for hyperthermia and promote to enhance the drug function [57-58]. Jing et al investigated the potential effects of combination therapy using Fe_3O_4 nanoparticles and chemotherapeutic drugs on lymphoma cells, and found that Fe_3O_4 nanoparticles and chemotherapeutic drugs interacted synergistically to induce apoptosis in lymphoma cells [57]. Xu et al. developed multimodal, magnetic C/Fe nanoparticles used as anticancer drug nanocarriers, as well as thermal agents under frequency excitation, and the results indicated that the DOX efficiency was enhanced to the high level of 3.5 fold increase in cellular death due to the heating by magnetic nanoparticles

[58]. Therefore, in this study, the Fe_3O_4/MBG/PCL scaffolds could synergistically enhance the efficiency of cancer treatment through the combination of magnetic hyperthermia with anticancer drug delivery, which could open up possibilities for the development of multifunctional and multi-therapeutic approaches for bone tumor treatment.

Although it is believed that magnetic Fe_3O_4 nanoparticles are inert, biocompatible nanomaterials capable of being eventually metabolized, they could be toxic to cells when its concentrations are more than 0.05 mg/L [59]. Investigation of cellular behavior on magnetic scaffolds indicated that the incorporation of Fe_3O_4 nanoparticles in MBG/PCL scaffolds did not lead to toxic effects. On the contrary, cells cultured on magnetic Fe_3O_4/MBG/PCL scaffolds showed better attachment and proliferation compared to the MBG/PCL scaffolds during the first week of cultivation (Fig. 7 and Fig. 8A), which indicated that the incorporation of Fe_3O_4 nanoparticles into the MBG/PCL scaffolds was beneficial for the growth of h-BMSCs. A recent study demonstrated that the Fe_3O_4 nanoparticles promoted cell growth due to its ability to diminish intracellular H_2O_2 through intrinsic peroxidase-like activity and Fe_3O_4 nanoparticles can also accelerate cell cycle progression [28]. Furthermore, our results showed that incorporation of Fe_3O_4 nanoparticles into MBG/PCL scaffolds stimulated ALP activity, osteogenic-related gene expression and ECM mineralization of h-BMSCs without exposure to an alternating magnetic field (Fig. 8-10). Similar results were reported in several previous studies on the osteoinductive effect of magnetic nanoparticles. Wu et al. showed that the integration of magnetic nanoparticles in Ca-P ceramics could promote the proliferation and differentiation of osteoblasts (Ros17⁄2.8 and MG63), and enhance the rhBMP-2 expression to accelerate the bone-like tissue formation [31]. Meng et

al demonstrated that the addition of magnetic nanoparticles in hydroxyapatite nanoparticles (nHA)/poly (D,L-lactide) (PLA) composite nanofibrous films that induce a significantly higher proliferation rate and faster differentiation of osteoblast cells [32]. It might be that each magnetic nanoparticle could be considered as a single magnetic domain with a tiny magnetic field. Once incorporation of Fe_3O_4 nanoparticles into the MBG/PCL scaffolds, the micro-environments in the pores or on the surface of the scaffolds were composed of a great number of tiny magnetic fields, and the total effect would likely be strengthened with an increase of the amount of Fe_3O_4 nanoparticles, which might affect the ion channels on the cell membrane and subsequently express osteoinductive effect under magnetic fields [60-61]. Therefore, the $5Fe_3O_4$/MBG/PCL, $10Fe_3O_4$/MBG/PCL and $15Fe_3O_4$/MBG/PCL scaffolds could provide a tiny static magnetic environment, which may contribute to the enhanced proliferation and differentiation of h-BMSCs on these magnetic scaffolds. Although the mechanism of h-BMSCs stimulation on magnetic Fe_3O_4/MBG/PCL scaffolds without exposure to an alternating magnetic field is not clear yet.

In this study the results indicated that the Fe_3O_4/MBG/PCL scaffolds are promising multifunctional platform with excellent bioactivity, osteogenic ability, local anticancer drug delivery and hyperthermia, which would be potential to reconstruct bone defect caused by bone tumor resection. Further studies will be conducted to investigate the effect of magnetic heating and drug delivery of the scaffolds on the behavior of cancer cells and osteoblast cells and in vivo studies.

5. Conclusions

In this study, 3D magnetic Fe_3O_4/MBG/PCL scaffolds with hierarchically meso-macropore architecture and uniform pore size and morphology were fabricated by a 3D printing technique. The Fe_3O_4/MBG/PCL scaffolds exhibited excellent apatite-forming bioactivity, sustained anticancer drug delivery and magnetic heating properties due to the mesoporous structure of MBG and Fe_3O_4 nanoparticles. Furthermore, the incorporation of Fe_3O_4 nanoparticles into the MBG/PCL scaffolds stimulated h-BMSCs' proliferation and differentiation. Therefore, the multifunctionality of the 3D printed magnetic Fe_3O_4/MBG/PCL scaffolds suggests that there is a great potential for their use in the treatment and regeneration of bone defects caused by bone tumors through a combination of enhanced osteogenic activity, local anticancer drug delivery and magnetic hyperthermia.

6. Acknowledgments

The authors gratefully acknowledge the support by the Program for Professor of Special Appointment (Eastern Scholar) at Shanghai Institutions of Higher Learning, National Natural Science Foundation of China (No. 51302170, 51242008, 81171738 and 81371936), Shanghai Nature Science Foundation (No.13ZR1458600), Innovation Program of Shanghai Municipal Education Commission (No. 14YZ085), and the Hujiang Foundation of China (No. B14006).

References:

[1] P. G. Carnesale and J. A. Pitcock, Tumors, 1980, 6, 1277-1378.

[2] J. M. Lane, E. Tomin and M. P. Bostrom, Clin Orthop Relat Res, 1999, S107-17.

[3] E. D. Arrington, W. J. Smith, H.G. Chambers, A. L. Bucknell and N. A. Davino, Clin Orthop

Relat Res , 1996, 300-309.

[4] J. C. Reichert, M. A. Woodruff, T. Friis, V. M. C. Quent, S. Gronthos, G. N. Duda, M. A. Schütz and D. W. Hutmacher, J Tissue Eng Regen Med, 2010, 4, 565-576.

[5] S. Reppenhagen, J. C. Reichert, L. Rackwitz, M. Rudert, P. Raab, G. Daculsi and U. Nöth, Int Orthop, 2012, 36, 139-148.

[6] D. W. Hutmacher, J. T. Schantz, C. X. F. Lam, K. C. Tan and T. C. Lim, J Tissue Eng Regen Med, 2007, 1, 245-260.

[7] J.-H. Bae, H.-R. Song, H.-J. Kim, H.-C. Lim, J.-H. Park, Y. Liu and S.-H. Teoh, Tissue Eng: Part A, 2011, 17, 2389-2397.

[8] S. J. Hollister, R. A. Levy, T.-M. Chu, J. W. Halloran, S. E. Feinberg, Int J Oral Maxillofac Surg, 2000, 29, 67-71.

[9] Q. Fu, E. Saiz and M.N. Raham, Mater Sci Eng C, 2011, 31, 1245-1256.

[10] F. Baino and C. Vitale-Brovarone, J Biomed Mater Res Part A, 2011, 97, 514-535.

[11] Y. Luo, C. Wu, A. Lode and M. Gelinsky, Biofabrication, 2013, 5, 015005.

[12] C. Wu, Y. Luo, G. Cuniberti, Y. Xiao and M. Gelinsky, Acta Biomater, 2011, 7, 2644-2650.

[13] I. Drosse, E. Volkmer, R. Capanna, P. D. Biase, W. Mutschler and M. Schieker, Injury, 2008, 39.

[14] X. Yan, X. Huang, C. Yu, H. Deng, Y. Wang and Z. Zhang, Biomaterials, 2006, 27, 3396-3403.

[15] X. Li, J. Shi, X. Dong, L. Zhang and H. Zeng, J Biomed Mater Res Part A, 2008, 84, 84-91.

[16] M. Alcaide, P. Portoles, A. Lopez-Noriega, D. Arcos, M. Vallet-Regi and M. T. Portoles, Acta Biomater, 2010, 6, 892-899.

[17] H. S. Yun, S. E. Kim, Y. T. Hyun, S. J. Heo and J. W. Shin, J Biomed Mater Res Part B, 2008, 87, 374-380.

[18] Y. Zhu and S. Kaskel, Micropor Mesopor Mater, 2009, 118, 176-182.

[19] C. Wu and J. Chang, Interface Focus, 2012, 2, 292-306.

[20] M. Manzano and M. Vallet-Regi, Progress Solid State Chem, 2012, 40, 17-30.

[21] S. Laurent, S. Dutz, U. O. Häfeli and M. Mahmoudi, Adv Colloid Interface Sci, 2011, 166, 8-23.

[22] C. S. S. R. Kumar and F. Mohammad, Adv Drug Del Rev, 2011, 63, 789-808.

[23] A. Amirfazli, Nature Nanotech, 2007, 2, 467-468.

[24] A. Ito, Y. Kuga, H. Honda, H. Kikkawa, A. Horiuchi and Y. Watanabe, Cancer Lett, 2004, 212, 167-175.

[25] M. J. Burfeindt, E. Zastrow, S. C. Hagness, B. D. Van Veen and J. E. Medow, Phy Med Biology, 2011, 56, 2743-2754.

[26] A. Matsumine, K. Kusuzaki, T. Matsubara, K. Shintani, H. Satonaka and T. Wakabayashi, Clin Exp Meta, 2007, 24, 191-200.

[27] B. Thiesen and A. Jordan, Int J Hyperthermia, 2008, 24, 467-474.

[28] D.-M. huang, J.-K. Hsiao, Y.-C. Chen, L.-Y. Chien, M. Yao, Y.-K. Chen, B.-S. Ko, S.-C. Hsu, L.-A. Tai, H.-Y. Cheng, S.-W. Wang, C.-S. Yang and Y.-C. Chen, Biomaterials, 2009, 30, 3645-3651.

[29] Y. Wei, X. Zhang, Y. Song, B. Han, X. Hu and X. Wang, Biomed mater, 2011, 6, 055008.

[30] N. Bock, A. Riminucci, C. Dionigi, A. Russo, A. Tampieri and E. Landi, Acta biomater, 2010, 6, 786-796.

[31] Y. Wu, W. Jiang, X. Wen, B. He, X. Zeng and G. Wang, Biomed mater, 2010, 5, 15001.

[32] J. Meng, Y. Zhang, X. Qi, H. Kong, C. Wang and Z. Xu, Nanoscale, 2010, 2, 2565-2569.

[33] J. Meng, B. Xiao, Y. Zhang, J. Liu, H. Xue and J. Lei, Scientific Rep, 2013, 3, 2655.

[34] R.L. Martin, G. Kristina, F. Thomas, K. Emanuel, D. Til and K. Stefan, Chem Commun, 2011, 47, 3075-3077.

[35] T. Kokubo and H. Takadama, Biomaterials, 2006, 27, 2907-2915.

[36] J. Zhang, S. Zhao, Y. Zhu, Y. Huang, M. Zhu, C. Tao and C. Zhang, Acta Biomater, 2014, 10, 2269-2281

[37] T. Matsubara, K. Suardita, M. Ishii, M. Sugiyama, A. Igarashi and R. Oda, J Bone Mineral Res, 2005, 20, 399-409.

[38] M. Lai, K. Cai, L. Zhao, X. Chen, Y. Hou and Z. Yang, Biomacromolecules, 2011, 12, 1097-1105.

[39] Y. P. He, S. Q. Wang, C. R. Li, Y. M. Miao, Z. Y. Wu, B. S. Zou, J Phys D: Appl Phys 2005, 38, 1342

[40] C. A llen, J. Han, Y. Yu, D. Maysinger and A. Eisenberg, J control Release, 2000, 63, 275-286.

[41] K. W. Ng, D. W. Hutmacher, J. T. Schantz, C. S. Ng, H. P. Too and T. C. Lim, Tissue Eng , 2001, 7, 441-455.

[42] D. W. Hutmacher, T. Schantz, I. Zein, K. W. Ng, S. H. Teoh and K. C. Tan, J Biomed Mater Res, 2001, 55, 203-216.

[43] F. Causa, E. Battista, M. R. Della, D. Guarnieri, M. Iannone and P. A. Netti, Langmuir, 2010, 26, 9875-9884.

[44] M. Vallet-Regi and E. Ruiz-Hernandez, Adv Mater, 2011, 23, 5177-5218.

[45] V. Mourino and A. R. Boccaccini, J Royal Society, 2010, 7, 209-227.

[46] M. Domingos, F. Intranuovo, A. Gloria, R. Gristina, L. Ambrosio, P. J. Bartolo and P. Favia, Acta Biomater, 2012, 9, 5997-6005.

[47] C. Loty, J. M. Sautier, H. Boulekbache, T. Kokubo, H. M. Kim and N. Forest, J Biomed Mater Res, 2000, 49, 423-434.

[48] D. Putnam, Nature Mater, 2008, 7, 836-837.

[49] R. D. Issels, J Eur Cancer, 2008, 44, 2546-2554.

[50] Y. Hong, X. Chen, X. Jing, H. Fan, Z. Gu and X. Zhang, Adv Fun Mater, 2010, 20, 1503-1510.

[51] M. Zhu, J. Shi, Q. He, L. Zhang, F. Chen and Y. Chen, J Mater Sci, 2012, 47, 2256-2263.

[52] D. Jańczewski, Y. Zhang, G. K. Das, D. K. Yi, P. Padmanabhan and K. K. Bhakoo, Micro Res Technol, 2011, 74, 563-576.

[53] J. P. Fortin, F. Gazeau and C. Wilhelm, J Eur Biophy, 2008, 37, 223-228.

[54] Y. Xu, M. Mahmood, A. Fejleh, Z. Li, F. Watanabe and S. Trigwell, Nanomedicine. 2010, 5, 167.

[55] L. G. Da, D. L. Zhou, Y. Lin, T. H. Pan, G. S. Chen and Q. D. Yin, Mater Sci Eng C, 2010, 30, 148-153.

[56] F. Matsuoka, M. Shinkai, H. Honda, T. Kubo, T. Sugita and T. Kobayashi, Biomagn Res Technol, 2004, 2, 3.

[57] H. Jing, J. Wang, P. Yang, X. Ke, G. Xia and B. Chen, Int J Nanomed, 2010, 5, 999-1004.

[58] Y. Xu, A. Karmakar, W. E. Heberlein, T. Mustafa, A. R. Biris and A. S. Biris, Adv Health

Mater, 2012, 1, 493-501.

[59] M. Mahmoudi, A. Simchi, A. Milani and P. Stroeve, J Col Inter sci, 2009, 336, 510-518.

[60] S. Hughes, A. J. ElHaj and J. Dobson, Med Eng Phy, 2005, 27, 754-762.

[61] J. F. Shen, Y. L. Chao and L. Du, Neurosci Lett, 2007, 415, 164-168.

Table 1 The compositions, porosity, compressive strength and magnetic heating properties (180G-409KHz) of the scaffolds.

Samples	Fe_3O_4 (Wt %)	MBG (Wt %)	PCL (Wt %)	Porosity (%)	compressive strength (MPa)	SAR (W/g)
MBG/PCL	0	61.5	38.5	59.6±5.6	13.1±1.6	0
5 Fe_3O_4/MBG/PCL	3.1	58.4	38.5	62.9±6.7	13.9±1.4	1.4
10Fe_3O_4/MBG/PCL	6.2	55.3	38.5	61.7±5.4	15.7±4.0	2.9
15Fe_3O_4/MBG/PCL	9.3	52.3	38.5	61.7±5.4	16.6±1.9	4.7

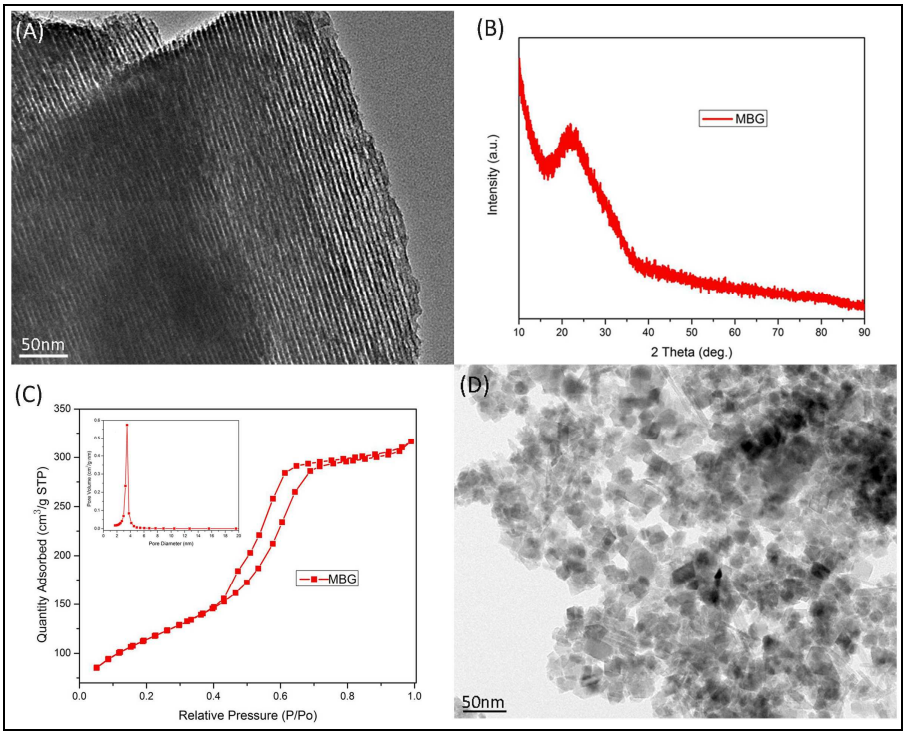

Fig.1 (A) TEM image, (B) wide-angle XRD pattern and (C) N_2 adsorption-desorption isotherm of MBG powders (insert: the corresponding pore size distribution of MBG powders); (D) TEM image of Fe_3O_4 nanoparticles.

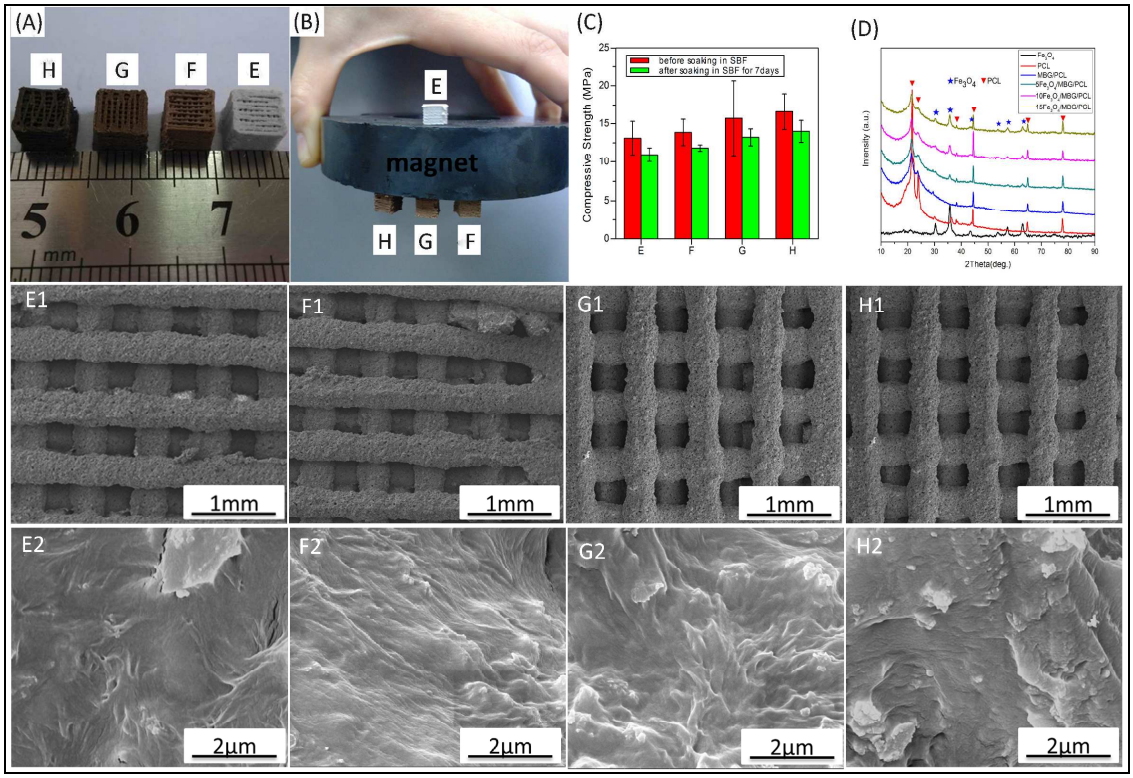

Fig. 2 (A) Photograph of the (E) MBG/PCL, (F) $5Fe_3O_4$/MBG/PCL, (G) $10Fe_3O_4$/MBG/PCL and (H) 15 Fe_3O_4/MBG/PCL scaffolds printed by 3D Bioplotter™; (B) Photograph for showing the attraction of the Fe_3O_4/MBG/PCL scaffolds to a standard magnet; (C) Compressive strength of (E) MBG/PCL, (F) $5Fe_3O_4$/MBG/PCL, (G) $10Fe_3O_4$/MBG/PCL and (H) $15Fe_3O_4$/MBG/PCL scaffolds before and after soaking in SBF for 7 days; (D) Wide-angle XRD patterns of magnetic Fe_3O_4 nanoparticles, polycaprolactone (PCL), MBG/PCL, $5Fe_3O_4$/MBG/PCL, $10Fe_3O_4$/MBG/PCL and $15Fe_3O_4$/MBG/PCL scaffolds. SEM images for the MBG/PCL (E1 and E2), $5Fe_3O_4$/MBG/PCL (F1 and F2), $10Fe_3O_4$/MBG/PCL (G1 and G2) and $15Fe_3O4$/MBG/PCL (H1 and H2) scaffolds. Magnification: ×100 for E1, F1, G1 and H1; ×50,000 for E2, F2, G2 and H2.

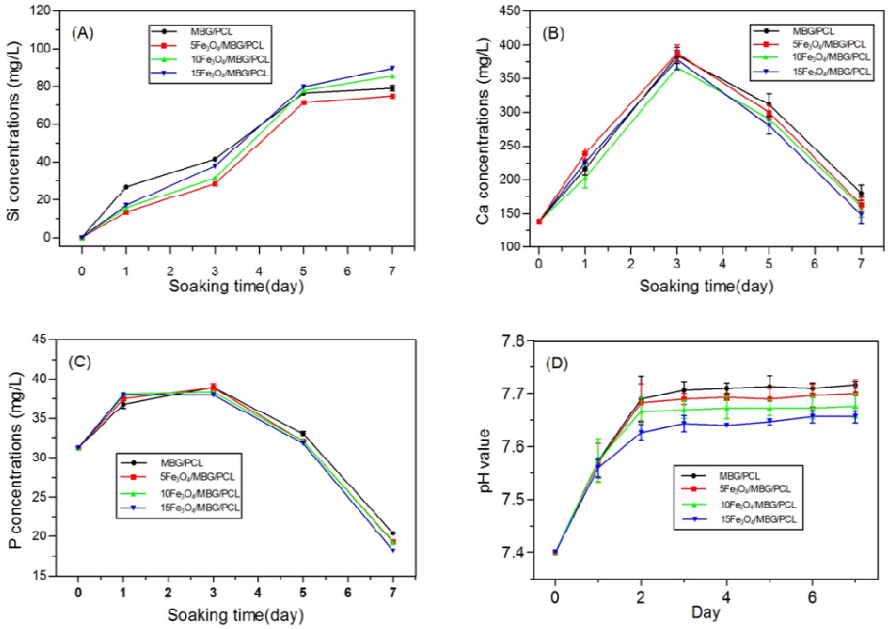

Fig.3 (A) Si, (B) Ca and (C) P ion concentrations in SBF solutions and (D) pH values of SBF solutions after soaking the MBG/PCL and Fe_3O_4/MBG/PCL scaffolds for various time periods.

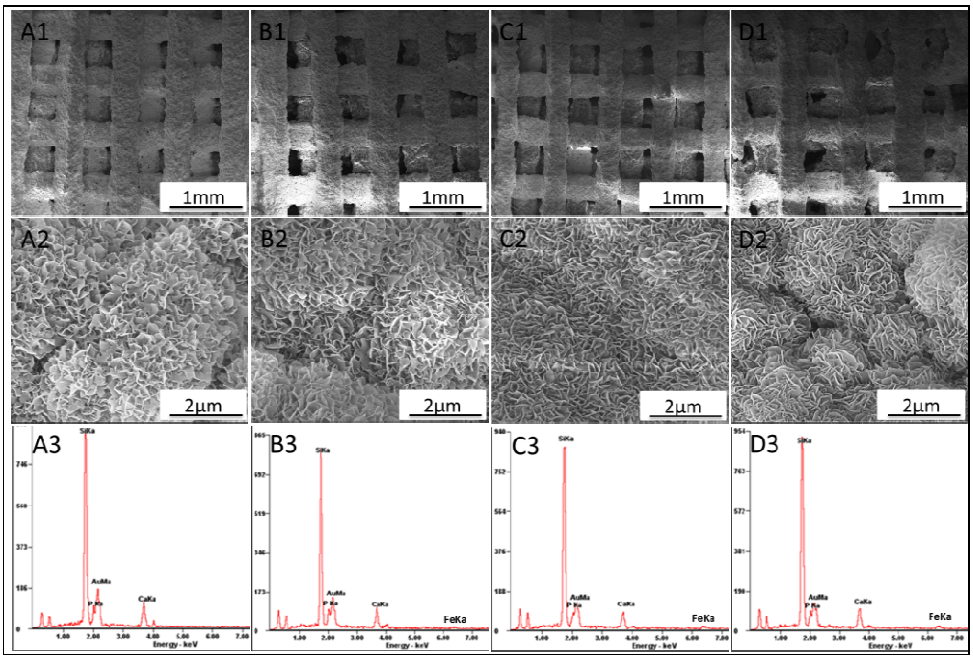

Fig.4 SEM images for the MBG/PCL(A1 and A2), $5Fe_3O_4$/MBG/PCL(B1 and B2), $10Fe_3O_4$/MBG/PCL (C1 and C2) and $15Fe_3O_4$/MBG/PCL (D1 and D2) scaffolds after soaking in SBF for 3 days; EDS analysis for the MBG/PCL (A3), $5Fe_3O_4$/MBG/PCL (B3), $10Fe_3O_4$/MBG/PCL (C3) and $15Fe_3O4$/MBG/PCL (D3) scaffolds after soaking in SBF for 3 days. Magnification: ×100 for A1, B1, C1 and D1; ×50,000 for A2, B2, C2 and D2.

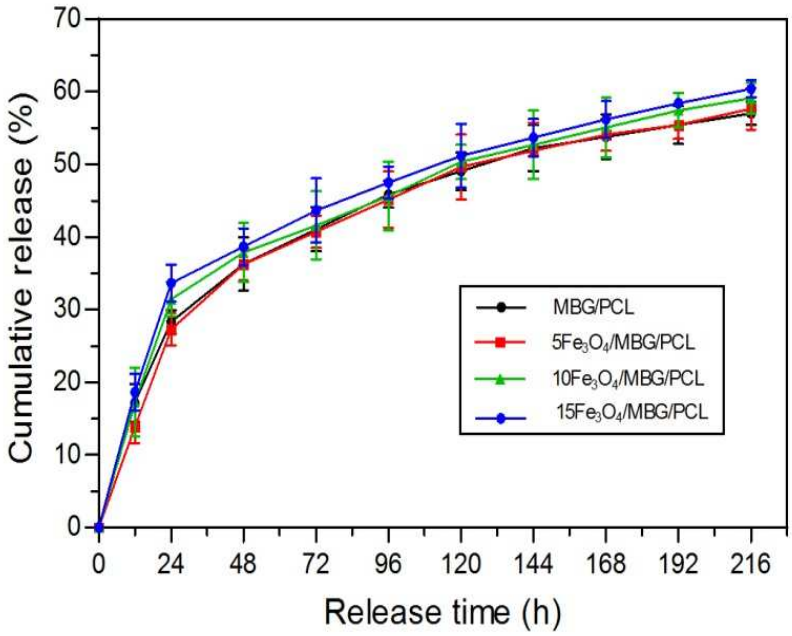

Fig.5 DOX release profiles from the MBG/PCL and Fe_3O_4/MBG/PCL scaffolds in SBF at 37 ^{o}C.

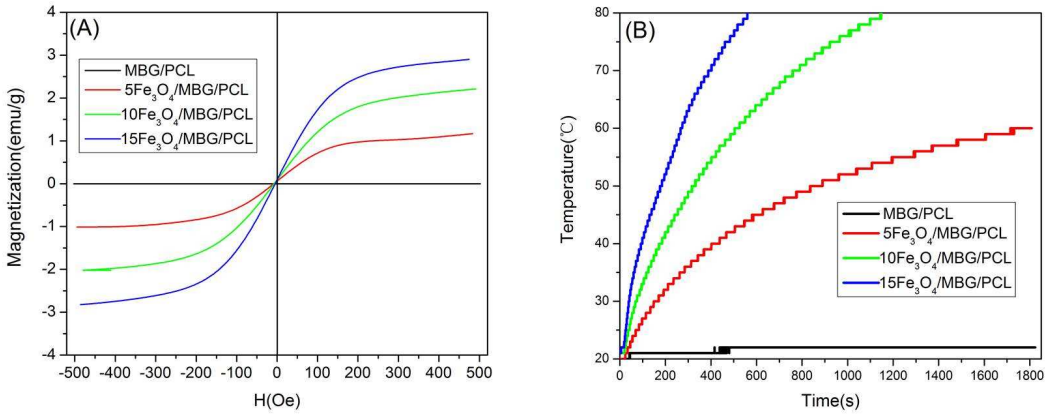

Fig.6 (A) Magnetization curves measured at 300 K and (B) changes in the solution temperature (magnetic strength of 180G and AC frequency of 409 kHz) of the MBG/PCL and Fe_3O_4/MBG/PCL scaffolds.

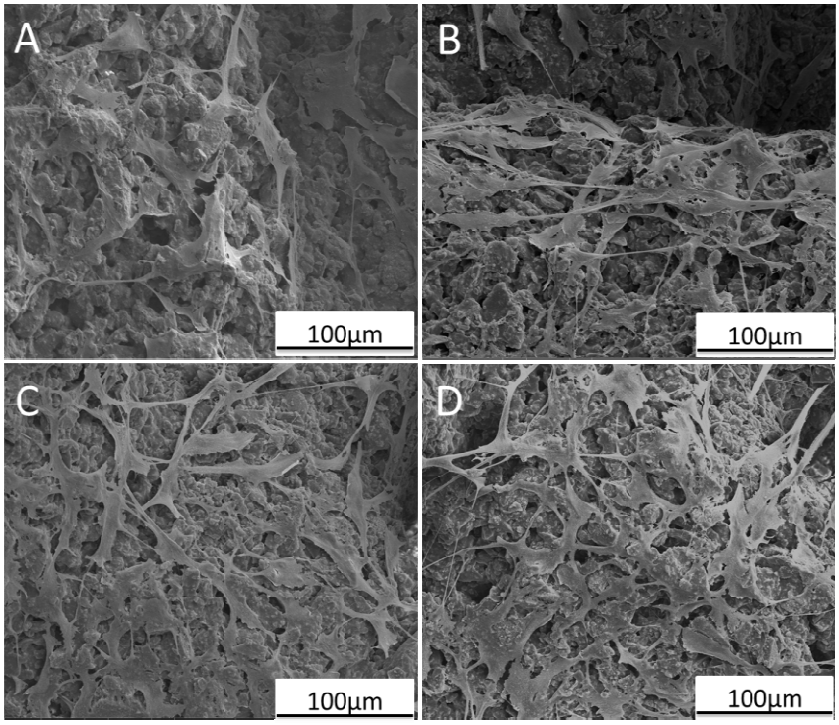

Fig.7 SEM images of the attachment of h-BMSCs cells on the MBG/PCL (A), 5 Fe_3O_4/MBG/PCL (B), 10Fe_3O_4/MBG/PCL (C) and 15Fe_3O_4/MBG/PCL (D) scaffolds after culturing for 7 days.

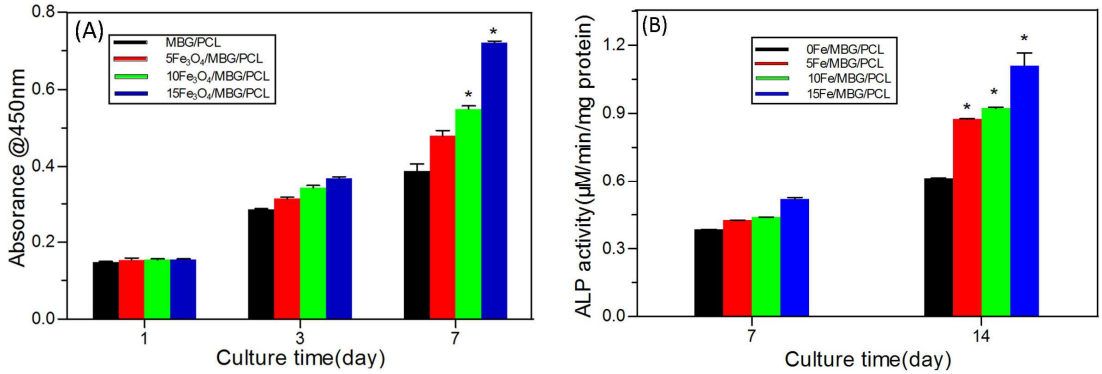

Fig.8 (A) The proliferation of h-BMSCs cells cultured on the MBG/PCL, $5Fe_3O_4$/MBG/PCL, $10Fe_3O_4$/MBG/PCL and $15Fe_3O_4$/MBG/PCL scaffolds for1, 3 and 7 days (n=4, *P<0.05); (B) The ALP activity of h-BMSCs cells cultured on the MBG/PCL, $5Fe_3O_4$/MBG/PCL, $10Fe_3O_4$/MBG/PCL and $15Fe_3O_4$/MBG/PCL scaffolds for 7 and 14 days (n=4, *P<0.05).

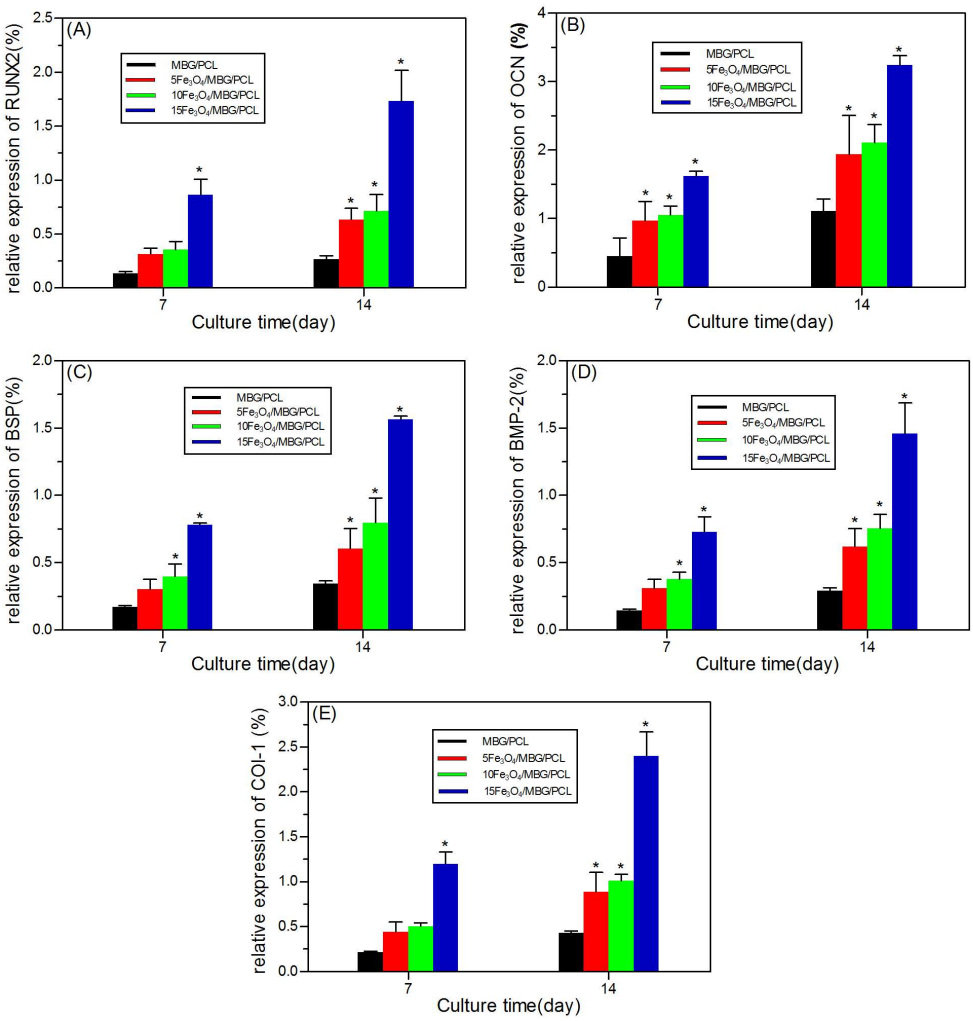

Fig.9 Osteogenic expression of RUNX2 (A), OCN (B), BSP (C), BMP-2 (D) and COL-1 (E) for h-BMSCs cells cultured on MBG/PCL, $5Fe_3O_4$/MBG/PCL, $10Fe_3O_4$/MBG/PCL and $15Fe_3O_4$/MBG/PCL scaffolds by qRT-PCR analysis after 7 and 14 days (n=4, *P<0.05).

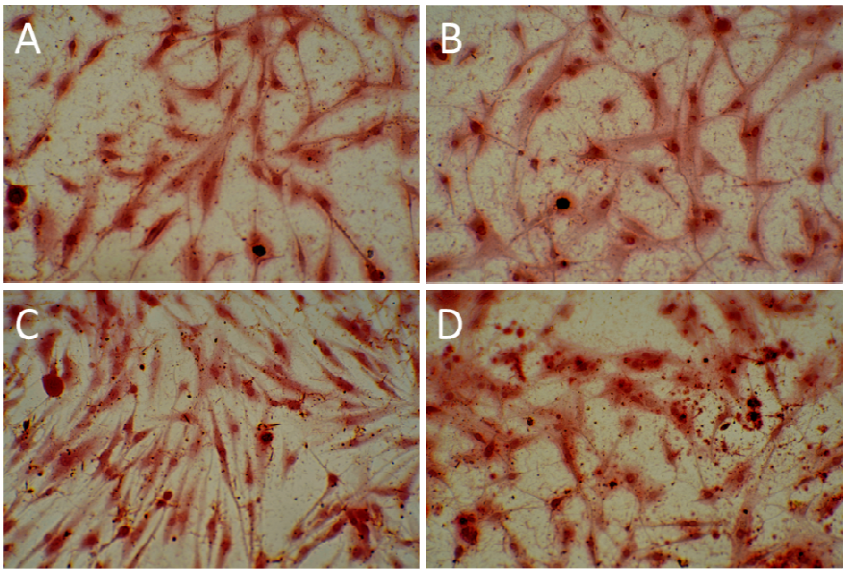

Fig.10 ECM mineralization of h-BMSCs cells on the MBG/PCL(A), 5Fe_3O_4/MBG/PCL(B), 10Fe_3O_4/MBG/PCL(C) and 15Fe_3O_4/MBG/PCL(D) scaffolds after culturing for 14 days using the Alizarin red S assay.

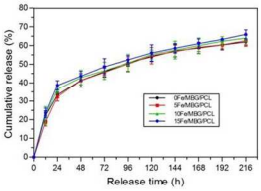

Sustained drug release

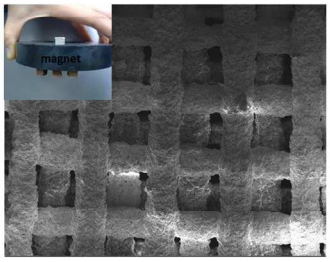

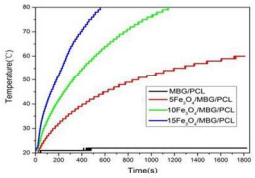

Temperature change

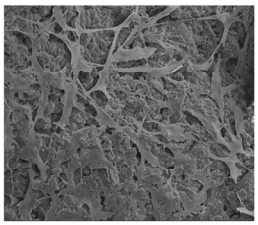

Cell attachment

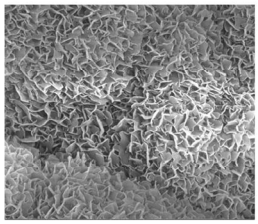

Apatite formation

The 3D-printed Fe3O4/MBG/PCL scaffolds with multifunctionality of enhanced osteogenic activity, local anticancer drug delivery and magnetic hyperthermia would be promising for use in the treatment and regeneration of large bone defects after tumor resection.
279x189mm (150 x 150 DPI)